

Multifunctional Polyoxometalate-Platforms for Supramolecular Light-driven Hydrogen Evolution

Salam Maloul,^{*} Matthias van den Borg,[†] Carolin Müller,^{§¶} Linda Zedler,[¶] Alexander Mengele,^{*} Daniel Gaissmaier,^{†¶‡} Timo Jacob,^{†¶‡*} Sven Rau^{**} Benjamin Dietzek-Ivanšić^{§¶*} and Carsten Streb^{**}

^{*}Institute of Inorganic Chemistry I, Ulm University, Albert-Einstein-Allee 11, 89081 Ulm, Germany

E-mail: sven.rau@uni-ulm.de; carsten.streb@uni-ulm.de

[†] Institute of Electrochemistry, Ulm University, Albert-Einstein-Allee 47, 89081 Ulm, Germany

E-mail: timo.jacob@uni-ulm.de

[§] Institute of Physical Chemistry, Friedrich Schiller University Jena, Helmholtzweg 4. 07743 Jena, Germany

Email: benjamin.dietzek@uni-jena.de

[¶] Leibniz Institute of Photonic Technologies (IPHT), Albert-Einstein-Straße 9, 07745 Jena, Germany

[¶] Helmholtz-Institute Ulm (HIU) Electrochemical Energy Storage, Helmholtzstr. 11, 89081 Ulm, Germany

[‡] Karlsruhe Institute of Technology (KIT) P.O. Box 3640, 76021 Karlsruhe, Germany

KEYWORDS Polyoxometalate; Supramolecular; Hydrogen Evolution; Self-Assembly; Organic-Inorganic Hybrid

ABSTRACT: Multifunctional supramolecular systems are a central research topic in light-driven solar energy conversion. Here, we report a polyoxometalate (POM)-based supramolecular dyad, where two platinum-complex hydrogen evolution catalysts are covalently anchored to an Anderson polyoxomolybdate anion. Supramolecular electrostatic coupling of the system to an iridium photosensitizer enables visible light-driven hydrogen evolution. Combined theory and experiment demonstrate the multifunctionality of the POM, which acts as photosensitizer / catalyst-binding-site and facilitates light-induced charge-transfer and catalytic turnover. Chemical modification of the Pt-catalyst site leads to increased hydrogen evolution reactivity. Mechanistic studies shed light on the role of the individual components and provide a molecular understanding of the interactions which govern stability and reactivity. The system could serve as a blueprint for multifunctional polyoxometalates in energy conversion and storage.

Introduction

Supramolecular systems combine molecular-level control of structure and reactivity with the ability to deploy a range of specific intermolecular interactions to access new function. These concepts have led to groundbreaking developments ranging from supramolecular surface patterning¹ to molecular machines² and stimuli-responsive nanostructures.³ In the field of catalysis, supramolecular concepts have been developed to tune reactivity, selectivity as well as *in-situ* catalyst assembly,^{4,5} highlighting the enormous potential of this field of research. Over the last decade, pioneering studies have demonstrated the potential of supramolecular catalysis for energy conversion and storage,^{6,7} e.g. in the fields of water oxidation,^{8,9} CO₂ reduction,¹⁰ and the hydrogen evolution reaction (HER).^{11,12} In light-driven HER catalysis, pioneering studies have demonstrated how supramolecular systems can be accessed by combining molecular catalysts with molecular photosensitizers. Often, component interactions are controlled by electrostatics, hydrogen bonding or π -stacking.¹³⁻¹⁵

The design of molecular platforms is a central concept in supramolecular energy conversion, including HER, as it enables the merging of several functions in one molecule. So-called photochemical dyads utilize these concepts to combine photosensitizer, charge-transfer system and HER catalyst in one (supra)molecular assembly.¹⁶

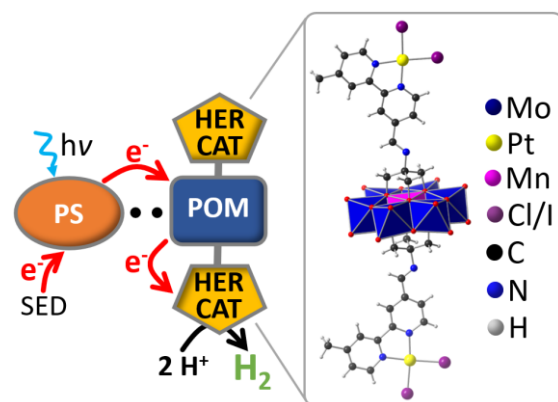


Figure 1: **Left:** Schematic illustration of the supramolecular photochemical system for visible light-driven hydrogen evolution. An anionic POM-platform molecule is covalently functionalized with a molecular Pt-HER catalyst. The system is electrostatically coupled to a cationic photosensitizer (PS). SED – sacrificial electron-donor. **Right:** molecular structure of the **POM-PtX**-platform (X = Cl, I, shown here: X = I, for crystallographic data see SI).

One classical approach is the linkage of molecular photosensitizer (e.g. Ru-^{14,17,18} or Ir-complexes) and metal complex catalysts (e.g. Pt-¹⁹ Pd-^{20,21} Rh-¹⁴ or Co-based^{15,18}) using ditopic bridging ligands for charge transfer.²² This has

led to unique models, where insights into the photophysical and electronic properties as well as HER activity have become possible using combined experiment and theory.^{14,17,22} This concept has been significantly expanded by recent studies where several photosensitizers were linked to HER catalytic sites, leading to operational supramolecular HER systems.^{23–25} Component optimization by chemical modification demonstrated the tunability of these systems, leading to in-depth understanding of function and reactivity limitations.^{14,19,21}

In recent years, the concept of supramolecular dyads has been expanded to the field of molecular metal oxides, or polyxometalates (POMs).²⁶ POMs are versatile dyad components, which can act as oxidation and reduction catalysts as well as charge separation²⁷ and charge-storage sites.^{28,29} In addition, their structure and reactivity can be tuned over a wide range by chemical modification.^{30–32} This versatility has made POMs a research focus for advanced, light-driven energy conversion and storage.^{29,33–35} In particular, the covalent organo-functionalization of POMs has paved the way for the design of multifunctional platform molecules,^{36,37} where several functions can in principle be incorporated in one POM.^{31,32,38,39} This has led to ground-breaking studies in light-driven hydrogen evolution,^{25,40} photo-electrochemistry²⁷ and nanocomposites for reversible electron storage.⁴¹ Building on these pioneering studies, we now propose the use of POMs as multifunctional redox-active platform molecules capable of charge storage, HER catalyst anchoring as well as supramolecular photosensitizer binding. Using this approach, multiple functions can be combined in one molecular assembly, while independent reactivity tuning would be possible by modification of each component.

Here, we report a new approach for supramolecular light-driven HER: an anionic Anderson-type platform-POM is covalently functionalized with a Pt(II)-complex HER catalyst. The compound is then electrostatically coupled in solution with a cationic iridium-photosensitizer (PS) to give the full supramolecular assembly. We demonstrate that in homogeneous solution, the system is capable of light-driven hydrogen evolution. Experimental and theoretical mechanistic studies show that the POM acts as PS- and catalyst-binding site, facilitating electron transfer under irradiation.

Results and Discussion

Catalyst synthesis and characterization

Briefly, the POM-platform molecules were synthesized in a one-pot reaction, where the 2,2'-bipyridine (bpy)-functionalized Anderson-anion precursor **POM-bpy** ($n\text{Bu}_4\text{N}$)₃[MnMo₆O₁₈{(OCH₂)₃CNCH(C₁₁H₉N₂)₂}₂]⁴⁰ was reacted with the respective Pt-precursor ([Pt(DMSO)₂Cl₂]⁴² or [Pt(DMSO)₂I₂]⁴³ in water-free, de-aerated acetonitrile to give the POM-catalyst systems **POM-PtCl** ($n\text{Bu}_4\text{N}$)₃[MnMo₆O₁₈{(OCH₂)₃CNCH(C₁₁H₉N₂)PtCl₂}₂] and **POM-PtI**

($n\text{Bu}_4\text{N}$)₃[MnMo₆O₁₈{(OCH₂)₃CNCH(C₁₁H₉N₂)PtI₂}₂], see SI for synthetic and analytical details. The solid, orange products were re-dissolved in N,N-dimethyl formamide (DMF), and diffusion of EtOAc into the DMF solution gave orange crystals suitable for single-crystal X-ray diffraction (scXRD). Yields: 70.2% (**POM-PtCl**), 76.4% (**POM-PtI**), yields based on Pt. **POM-PtCl** and **POM-PtI** were fully characterized by elemental analysis, NMR-, FT-IR-spectroscopy and scXRD,

see SI for details (CCDC reference numbers: 2099459 (**POM-PtCl**) and 2099460 (**POM-PtI**)). Note that when **POM-PtCl** and **POM-PtI** are discussed collectively, we will refer to them as **POM-PtX**.

Light-driven hydrogen evolution

The visible-light-driven HER activity of **POM-PtI** and **POM-PtCl** was examined using the photosensitizer [Ir(ppy)₂(bpy)]PF₆ (**PS**). **PS** was chosen due to its cationic charge, and the literature-known ability for light-driven electron transfer to POMs.^{25,44} In addition, (spectro-)electrochemical analyses of both **POM-PtX** species showed, that at least two electron transfers from the photoreduced **PS** ($E_{1/2}$ ca. -1.8 V vs. Fc⁺/Fc)⁴⁵ to **POM-PtX** is thermodynamically possible, as **POM-PtX** shows two redox-couples at potentials more positive than -1.8 V (see SI, Table S2, Figures S3, S4). Thus, light-driven catalytic studies were performed in water-free, de-aerated DMF solutions containing the respective catalyst **POM-PtX** (12.5 μM), the photosensitizer **PS** (125 μM) and triethyl amine/acetic acid (TEA (1.0 M) / HAc (0.2 M)) as sacrificial proton/electron donors; this experimental setup has been adapted from earlier POM-based HER studies.^{44,46–48} The samples were irradiated under an Ar atmosphere using monochromatic LEDs ($\lambda_{\text{max}} = 470$ nm, $P \sim 40$ mW cm⁻²) at 25°C. Hydrogen evolution was quantified by calibrated gas chromatography. Each data-point was recorded in triplicate, and averaged turnover numbers (*TONs*) are given based on the molar amount of Pt present, i.e., $TON = n(\text{H}_2) / n(\text{Pt})$. The non-modified catalysts [Pt(bpy)Cl₂] / [Pt(bpy)I₂] (25 μM) together with **PS** (125 μM) were used as references in control experiments. Also, control experiments without irradiation or in the absence of POM-catalysts show virtually no H₂ evolution (SI, Figure S5).

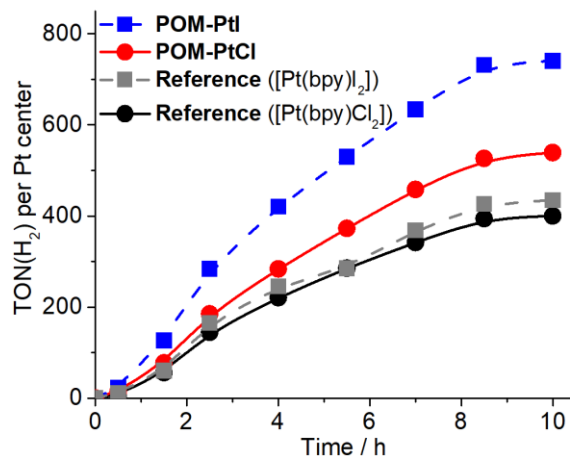


Figure 2 Light-driven HER activity of **POM-PtCl** (red), **POM-PtI** (blue) and the reference compounds [Pt(bpy)Cl₂] (black) and [Pt(bpy)I₂] (gray), showing the hydrogen evolution *TON* (calculated per Pt center) over time. Conditions: solvent: water-free, de-gassed DMF containing TEA (1.0 M) and HAc (0.2 M). $c(\text{POM-PtX}) = 12.5 \mu\text{M}$; $c([\text{Pt}(\text{bpy})\text{X}_2]) = 25 \mu\text{M}$, $c(\text{PS}) = 125 \mu\text{M}$, irradiation: LED, $\lambda_{\text{max}}=470$ nm, $P \sim 40$ mW cm⁻².

First, the HER activity of **POM-PtCl**, and the reference [Pt(bpy)Cl₂] were studied. It was observed that under irradiation H₂ evolution increases linearly with time for both

catalysts, see Fig. 2. After $t_{\text{irradiation}} = 10$ h, notable reactivity differences are observed. For **POM-PtCl** the $TONs$ reached ~ 540 , while for the reference $[Pt(bpy)Cl_2]$ only exhibits a TON of *ca.* 400.

To further enhance the activity of the catalyst, the chloride ions on the Pt centers were replaced with iodide to give the **POM-PtI** cluster (see synthetic discussion above for details). When employed for light-driven HER under identical conditions as described above, **POM-PtI** showed significantly higher activity with a maximum TON of *ca.* 740 after $t_{\text{irradiation}} = 10$ h (Figure 2). Note that the higher reactivity of **POM-PtI** compared with **POM-PtCl** is in line with previous reports: for the related compounds $[[Ru(tbbpy)_2(tpphz)PtX_2](PF_6)_2]$ ($X = Cl$ or I), a similar increase of HER activity is found when the chloride ligands are

replaced by iodides.¹⁹ The authors assigned this increased activity to the higher electron density at the Pt center due to the large, easily polarized iodide ligands.¹⁹ To the best of our knowledge, this is the first time that ligand-tuning concepts have been demonstrated in POM-based HER catalysis.

Based on the above data, we propose that the increased activity of **POM-PtCl** and **POM-PtI** compared to the non-covalently linked references is due to enhanced electrostatic attraction between the cationic PS and the anionic POM-catalyst. This could enable aggregation and charge-transfer in solution. To test this hypothesis, we performed a combined experimental and theoretical study which explores the interactions between PS and **POM-PtX**. Due to the higher reactivity, the study used **POM-PtI** as model.

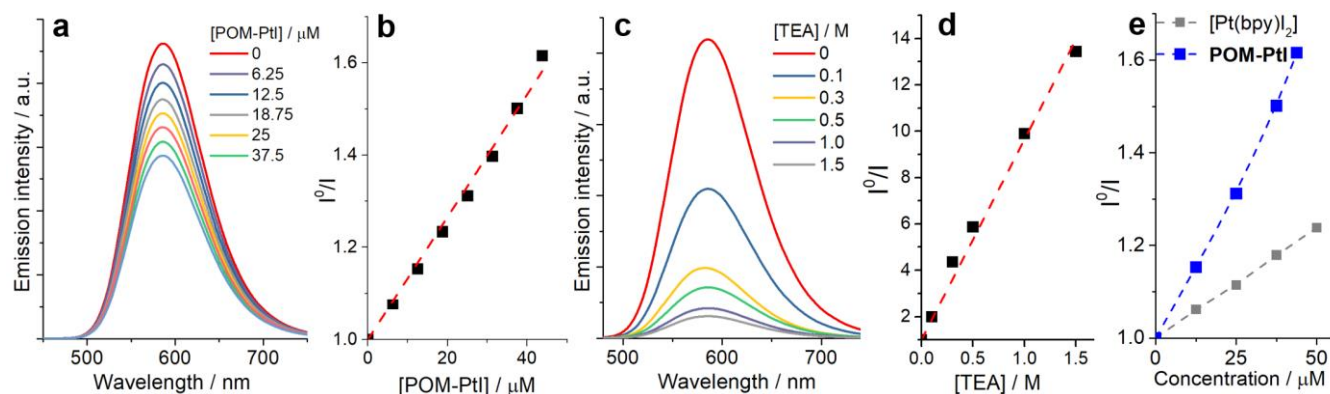


Figure 3 (a) Emission quenching spectra of PS $[[Ir(ppy)_2(bpy)]^+$, 125 μM) as a function of **[POM-PtI]**, and (b) corresponding Stern-Volmer plot; (c) emission quenching spectra of PS $[[Ir(ppy)_2(bpy)]^+$, 125 μM) as a function of [TEA], and (d) corresponding Stern-Volmer plot; (e) Stern-Volmer plot, comparing the emission quenching of PS by **POM-PtI** and the $[Pt(bpy)I_2]$ reference. Conditions: water-free, de-aerated DMF, details see SI, Section 7.

Mechanistic photophysical studies

To assess the supramolecular interactions between photosensitizer and catalyst, we examined the emission quenching of PS by the electron acceptor **POM-PtI** or the sacrificial electron donor TEA (Figure 3a-d).⁴⁹ The steady-state emission spectra and emission lifetimes of PS ($\lambda_{\text{excitation}} = 420$ nm) were measured upon addition of TEA or **POM-PtI** to a DMF of PS solutions (see Figure 3a,c and SI, Figure S7). The corresponding Stern-Volmer plots (Figure 3b,d and SI, Figures S7, S8) are analyzed by linear fitting resulting in quenching rate constants (k_q) of $7.1 \times 10^7 M^{-1}s^{-1}$ (reductive quenching, TEA) and $8.4 \times 10^{10} M^{-1}s^{-1}$ (oxidative quenching, **POM-PtI**). The calculated mutual diffusion rate constants (k_D) in DMF are $7.7 \times 10^9 M^{-1}s^{-1}$ (for PS/TEA) and $8.2 \times 10^9 M^{-1}s^{-1}$ (for PS/**POM-PtI**), respectively (see SI, Section 7). Comparison between k_D and k_q however shows that for reductive quenching (PS*/TEA) k_D is ~ 100 times higher than k_q , indicating a quenching efficiency per encounter of *ca.* 1%.⁵⁰ In contrast, for the oxidative quenching (PS*/**POM-PtI**) k_D is ~ 10 times smaller than k_q , indicating a quenching efficiency per encounter of formally $>100\%$. Two interpretations are in line with these observations: (a) the interactions of the PS cation and the **POM-PtI** anion increase the rate of interaction beyond the frequency calcu-

lated for neutral reaction partners within the Collins-Kimball model (see SI, Section 7);⁵¹ (b) a supramolecular pre-assembly of cationic PS and anionic **POM-PtI** enables PS* quenching at significantly faster rates than the mutual diffusion, *i.e.*, in the limit of static quenching.⁵² As a result, the oxidative quenching of PS* has to occur *via* both, static and dynamic quenching.

Next, the quenching efficiency of PS by the anionic **POM-PtI** was compared with the quenching behavior of the charge-neutral $[Pt(bpy)I_2]$ reference (Figure 3e). Here, **POM-PtI** showed a significantly higher quenching efficiency compared to the reference compound. This supports the suggestion that electrostatic attraction of PS and **POM-PtI** in solution can be used to enhance electronic interactions of the reaction partners following photoexcitation of the PS. This observation also supports the HER catalytic findings, where **POM-PtI** shows significantly higher reactivity than the $[Pt(bpy)I_2]$ reference (Figure 2).

Theoretical studies of PS / POM-PtI aggregation

To better understand the coupling between PS and **POM-PtCl** and its effects on the electronic properties of the system, first principles simulations using spin-polarized density functional theory (DFT) calculations within the ORCA program package.⁵³ Initial geometry optimization used the

PBEh-3c composite method⁵⁴ followed by geometry optimizations with the PBE0 hybrid functional^{55,56} and a def2-TZVP basis set.⁵⁷ For molybdenum and iridium, effective core potentials were used to replace the core electrons.^{58,59} Dispersion interactions were accounted for by atom-pairwise correction with the Becke–Johnson damping scheme [D3(BJ)].^{60,61} The conductor-like polarizable continuum model (CPCM) was used to implicitly include the DMF solvent ($\epsilon=38.30$ and $n=1.43$).⁶² Electron densities were analyzed by Hirshfeld population analysis to determine atomic charges.⁶³

To gain insights into the energetics and binding behavior of **PS** and **POM-PtX**, we used DFT calculations to assess the interaction energies between both species. As model systems, we focused on **PS** (charge: 1+) and **POM-PtCl** (charge: 3-), see Figure 4. As references, we studied [Pt(bpy)Cl₂] (charge-neutral) and the TRIS-functionalized prototype Anderson anion [MnMo₆O₁₈{(CH₂O)₃CNH₂}₂]³⁻ (**POM-Ref**, charge: 3-, SI, Figure S9).⁴⁰ Initial studies gave interaction energies of -48 kJ/mol (**PS** / [Pt(bpy)Cl₂]) and -76 kJ/mol (**PS** / **POM-ref**) and -77 kJ/mol (**PS** / **POM-PtCl**), respectively. This highlights, that supramolecular aggregation in solution between photosensitizer and POM is thermodynamically favored. For the **PS** / **POM-PtCl** system, we observe that in the energetically most favored system, **PS** is located next to the metal oxo cluster (Figure 4), highlighting the importance of the POM for **PS**-binding. Note that quantitatively virtually identical results were obtained for **POM-PtI**; these are shown in the SI, Section 8).

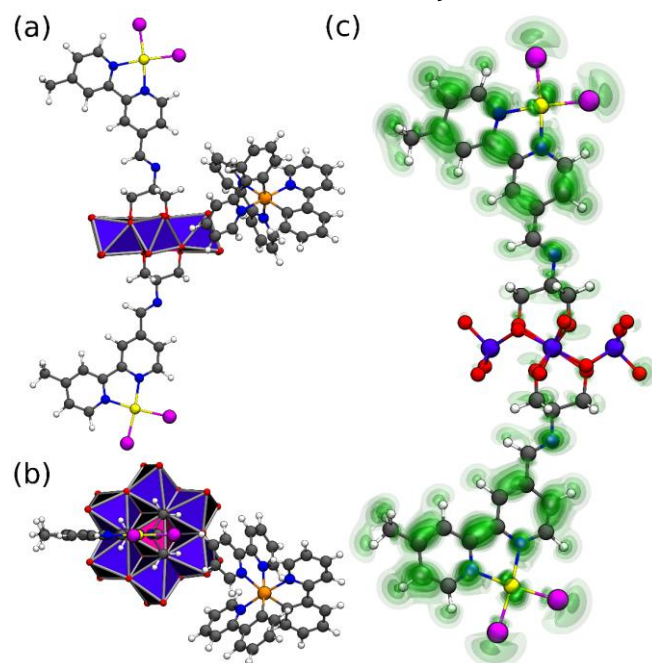


Figure 4: Energetically most favoured interaction sites between **PS** and **POM-PtI** in (a) side view and (b) top view; (c) representation of the f^+ Fukui function calculated for the one-electron-reduced **POM-PtCl**, shown as charge-difference plot. The iso-surfaces correspond to electron-accepting regions where an additional added electron will be located (as indicated by the f^+ Fukui function). Regions with higher values are marked in darker shades of green. Molecular colour scheme, see Figure 1.

Next, we theoretically assessed the electronic consequences of an electron-transfer from **PS** to **POM-PtCl**, which is a key redox step of the HER catalytic cycle. To this end, single-point calculations were performed on the one-electron reduced **POM-PtCl** as well as the one-electron reduced reference systems (*i.e.*, [Pt(bpy)Cl₂] and **POM-ref**). This allowed us to compare the Hirshfeld net charges of the one-electron reduced systems with the charge-distribution of the non-reduced systems. Note that this procedure is analogous to determining condensed Fukui functions.^{64,65} While Fukui functions are often used as descriptors for the chemical reactivity of a molecule (with respect to its electrophilic and nucleophilic regions), here, the function for a nucleophilic attack will serve as a measure for the uptake and distribution of additional electron density in the systems studied. The Fukui function f^+ is given by the difference between the electron densities of the initial state $\rho(N)$ and the state featuring one additional electron $\rho(N+1)$:

$$f^+ = \rho(N+1) - \rho(N)$$

The corresponding condensed Fukui function f_k^+ is defined as:

$$f_k^+ = q_k(N+1) - q_k(N)$$

where $q_k(N)$ describes the atomic charges at the respective atomic center k of the original system and $q_k(N+1)$ those of the system with one additional electron. After normalization, this provides a percentage value of the additional electron density at any given atom. For clarity, we have combined the resulting atomic percentages into three molecular sub-units, *i.e.* the 2,2'-bipyridine ligands (bpy), the platinum-chloride fragment {PtCl₂} and the POM metal-oxo framework {MnMo₆O₂₄}, see Table 1 and SI, Section 8 for computational details.

Table 1. Percentage distribution of an additional electron taken up by **POM-PtCl**, **POM-Ref** and [Pt(bpy)Cl₂] as calculated using normalized nucleophilic Fukui functions and Hirshfeld population analysis.

Fragment	POM-PtCl	POM-Ref	[Pt(bpy)Cl ₂]
bpy	75.5	-	79.7
{PtCl ₂ }	18.8	-	20.3
{MnMo ₆ O ₂₄ }	5.7	88.6	-

As shown in Table 1, analysis of the nucleophilic Fukui function for the one-electron reduced **POM-PtCl** indicates that additional electron density will be distributed on the Pt-HER catalyst, either on the {PtCl₂} fragment (18.8 %) or the bpy ligand (75.5 %), while only a low percentage of the additional electron is distributed on the POM framework (5.7 %). For the reference systems, the expected distributions are observed: in **POM-Ref**, 88.6 % of the electron density is located on the POM framework, while in [Pt(bpy)Cl₂], 79.7 % are located on the bpy and 20.3 % on the {PtCl₂} frag-

ment (Figure 4 and SI, Table S3). This is in line with experimental electrochemical and spectro-electrochemical data, which indicate that an electron transfer to the one-electron-reduced **POM-PtX**, *i.e.*, a second reduction of **POM-PtX** occurs on the {PtX(bpy)} moiety (SI, Figures S3, S4).

Reusability and stability of the molecular catalyst:

Finally, we were interested in understanding the causes of the loss of HER activity observed after ~ 9 h of irradiation (Figure 1). We hypothesized (based on initial UV-Vis spectroscopy of the reaction solution, SI, Figures S10, S11), that this could be due to **PS** degradation, and thus, loss of the light-harvesting capabilities of the system. To experimentally probe this, we performed a reusability experiment where the standard photochemical experiment (identical to the experiment shown in Figure 1, catalyst: **POM-PtI**) was performed. After 10 h of irradiation, an aliquot of fresh **PS** (110 μ M) was added to the reaction mixture and irradiation was resumed. As illustrated in Figure 5, the system resumed hydrogen evolution at high reactivity. This observation provides evidence that **PS** degradation is a major factor in reactivity loss in the system described, while catalytic activity by the **POM-PtI** is still observed. Thus, future studies can explore the design of more robust photosensitizers with optimized POM binding behavior.⁶⁶

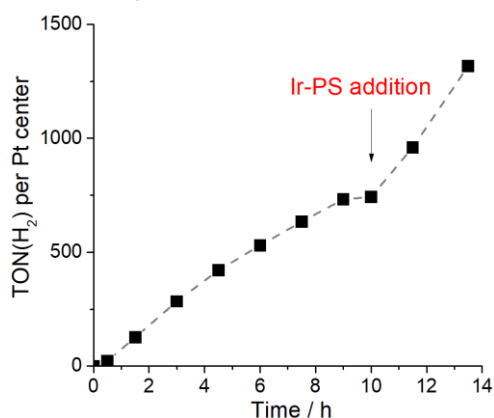


Figure 5 Reusability of the catalyst **POM-PtI** demonstrated by adding an aliquot of **PS** after HER activity ceased (after $t_{\text{irradiation}} = 10$ h). Conditions are identical to the HER experiments shown in Figure 1.

To gain further insight into the stability of **POM-PtX**, we performed a range of mechanistic analyses: First, UV-Vis spectroscopy of **POM-PtX** in the reaction solvent DMF showed no spectral changes over 18 h (SI, Figure S11). Also, microfiltration and UV-Vis spectroscopic analysis of a reaction mixture containing **POM-PtI** and **PS** (molar ratio: 1/10) showed no spectral changes, indicating that no colloidal particles are observed (SI, Figure S12). This was supported by dynamic light scattering (DLS) on the catalytic reaction solution, where no particles within the measurement range (1 – 10000 nm) were detected. This suggests that the system does not produce colloidal platinum particles as the active HER catalyst, but that a molecular system operates as HER catalyst in the present study. Note that the “classical” mercury amalgam test for Pt colloids was not suitable for

the present system, as elemental Hg undergoes redox-reactions with **POM-PtX** already in the dark, resulting in fast degradation of the **POM-PtX** molecule. Similar behavior has been reported before.¹⁹

To provide further evidence for the molecular nature of the HER system reported, we performed a catalytic experiment under the standard conditions described in Figure 1 using **POM-PtCl** as model catalyst. Then, excess *n*Bu₄NI was added to the reaction solution to trigger iodide-for chloride ligand exchange on **POM-PtCl** (leading to partial *in-situ* formation of **POM-PtI**). As predicted from our initial experiments (Figure 1), this led to an increase of the TON (+ ~ 20 %), thereby providing further evidence of a molecular HER catalysis (SI, Figure S13).^{67,68}

Conclusion

In sum, we demonstrate how organo-functionalized polyoxometalates can be used as multifunctional platforms for supramolecular light-driven hydrogen evolution catalysis. Electrostatic solution-interactions between an anionic, Pt-functionalized POM dyad with a cationic photosensitizer lead to light-driven charge-transfer and H₂ evolution in solution. The reactivity of the dyads surpasses the purely intermolecular reference systems, and reactivity tuning of the dyads is possible by ligand exchange. Experiment and theory shed light on the underlying interactions in solution, and initial stability analyses highlight future areas of development. Our results open new avenues for the design of supramolecular light-driven hydrogen evolution catalysis.

ASSOCIATED CONTENT

Supporting Information. Experimental, analytical and theoretical data are supplied.

AUTHOR INFORMATION

Corresponding Author

* Timo.Jacob: timo.jacob@uni-ulm.de; Benjamin Dietzek: Benjamin.dietzek@uni-jena.de; Sven Rau: sven.rau@uni-ulm.de; Carsten Streb: Carsten.streb@uni-ulm.de

Author Contributions

S.M. performed syntheses and catalytic studies. M.v.d.B., D.G. and T.J. performed theoretical analyses. C.M., L.Z. and B.D. performed photophysical analyses. A.M., T.J., S.R., B.D. and C.S. analyzed and interpreted data. All authors co-wrote the manuscript. All authors have given approval to the final version of the manuscript.

Funding Sources

Financial support by the Deutsche Forschungsgemeinschaft DFG through the Transregio-Collaborative Research Center TRR234 CataLight, project no 364549901, projects A1, A4 and A5 and the priority program SPP2102 *Light-controlled reactivity of metal complexes*, project no 359737763 is gratefully acknowledged. C.M. gratefully acknowledges support by the Fonds der Chemischen Industrie FCI through a Kekulé fellowship. S.M. gratefully acknowledges financial support by the

ACKNOWLEDGMENT

We gratefully acknowledge Ilse E. Friedländer for assistance with spectro-electrochemical measurements.

REFERENCES

- (1) Goronzy, D. P.; Ebrahimi, M.; Rosei, F.; Arramel, Fang, Y.; De Feyter, S.; Tait, S. L.; Wang, C.; Beton, P. H.; Wee, A. T. S.; et al. Supramolecular Assemblies on Surfaces: Nanopatterning, Functionality, and Reactivity. *ACS Nano* **2018**, *12* (8), 7445–7481. <https://doi.org/10.1021/acsnano.8b03513>.
- (2) Iino, R.; Kinbara, K.; Bryant, Z. (guest eds). Special Issue: Molecular Motors. *Chem. Rev.* **2020**, *120* (1), 1–460. <https://doi.org/10.1021/acs.chemrev.9b00819>.
- (3) Li, Z.; Song, N.; Yang, Y.-W. Stimuli-Responsive Drug-Delivery Systems Based on Supramolecular Nanovalves. *Matter* **2019**, *1* (2), 345–368. <https://doi.org/10.1016/j.matt.2019.05.019>.
- (4) Meeuwissen, J.; Reek, J. N. H. Supramolecular Catalysis beyond Enzyme Mimics. *Nat. Chem.* **2010**, *2* (8), 615–621. <https://doi.org/10.1038/nchem.744>.
- (5) Raynal, M.; Ballester, P.; Vidal-Ferran, A.; van Leeuwen, P. W. N. M. Supramolecular Catalysis. Part 1: Non-Covalent Interactions as a Tool for Building and Modifying Homogeneous Catalysts. *Chem. Soc. Rev.* **2014**, *43* (5), 1660–1733. <https://doi.org/10.1039/C3CS60027K>.
- (6) Zhang, B.; Sun, L. Artificial Photosynthesis: Opportunities and Challenges of Molecular Catalysts. *Chem. Soc. Rev.* **2019**, *48* (7), 2216–2264. <https://doi.org/10.1039/C8CS00897C>.
- (7) Keijer, T.; Bouwens, T.; Hessels, J.; Reek, J. N. H. Supramolecular Strategies in Artificial Photosynthesis. *Chem. Sci.* **2021**, *12* (1), 50–70. <https://doi.org/10.1039/D0SC03715J>.
- (8) Bonchio, M.; Syrgiannis, Z.; Burian, M.; Marino, N.; Pizzolato, E.; Dirian, K.; Rigodanza, F.; Volpato, G. A.; La Ganga, G.; Demitri, N.; et al. Hierarchical Organization of Perylene Bisimides and Polyoxometalates for Photo-Assisted Water Oxidation. *Nat. Chem.* **2019**, *11* (2), 146–153. <https://doi.org/10.1038/s41557-018-0172-y>.
- (9) Kunz, V.; Schmidt, D.; Röhr, M. I. S.; Mitrić, R.; Würthner, F. Supramolecular Approaches to Improve the Performance of Ruthenium-Based Water Oxidation Catalysts. *Adv. Energy Mater.* **2017**, *7* (16), 1602939. <https://doi.org/10.1002/aenm.201602939>.
- (10) Tamaki, Y.; Ishitani, O. Supramolecular Photocatalysts for the Reduction of CO₂. *ACS Catal.* **2017**, *7* (5), 3394–3409. <https://doi.org/10.1021/acscatal.7b00440>.
- (11) Gärtner, F.; Sundararaju, B.; Surkus, A. E.; Boddien, A.; Loges, B.; Junge, H.; Dixneuf, P. H.; Beller, M. Light-Driven Hydrogen Generation: Efficient Iron-Based Water Reduction Catalysts. *Angew. Chem. Int. Ed.* **2009**, *48* (52), 9962–9965. <https://doi.org/10.1002/anie.200905115>.
- (12) Neubauer, A.; Grell, G.; Friedrich, A.; Bokarev, S. I.; Schwarzbach, P.; Gärtner, F.; Surkus, A.-E.; Junge, H.; Beller, M.; Kühn, O.; et al. Electron- and Energy-Transfer Processes in a Photocatalytic System Based on an Ir(III)-Photosensitizer and an Iron Catalyst. *J. Phys. Chem. Lett.* **2014**, *5* (11), 1355–1360. <https://doi.org/10.1021/jz5004318>.
- (13) Whang, D. R.; Park, S. Y. Rational Design of an Electron-Reservoir Pt(II) Complex for Efficient Photocatalytic Hydrogen Production from Water. *ChemSusChem* **2015**, *8* (19), 3204–3207. <https://doi.org/10.1002/cssc.201500787>.
- (14) White, T. A.; Whitaker, B. N.; Brewer, K. J. Discovering the Balance of Steric and Electronic Factors Needed To Provide a New Structural Motif for Photocatalytic Hydrogen Production from Water. *J. Am. Chem. Soc.* **2011**, *133* (39), 15332–15334. <https://doi.org/10.1021/ja206782k>.
- (15) Dong, J.; Wang, M.; Zhang, P.; Yang, S.; Liu, J.; Li, X.; Sun, L. Promoting Effect of Electrostatic Interaction between a Cobalt Catalyst and a Xanthene Dye on Visible-Light-Driven Electron Transfer and Hydrogen Production. *J. Phys. Chem. C* **2011**, *115* (30), 15089–15096. <https://doi.org/10.1021/jp2040778>.
- (16) Balzani, V.; Credi, A.; Venturi, M. Photochemical Conversion of Solar Energy. *ChemSusChem* **2008**, *1* (1–2), 26–58. <https://doi.org/10.1002/cssc.200700087>.
- (17) Tschierlei, S.; Karnahl, M.; Presselt, M.; Dietzek, B.; Guthmüller, J.; González, L.; Schmitt, M.; Rau, S.; Popp, J. Photochemical Fate: The First Step Determines Efficiency of H₂ Formation with a Supramolecular Photocatalyst. *Angew. Chem. Int. Ed.* **2010**, *49* (23), 3981–3984. <https://doi.org/10.1002/anie.200906595>.
- (18) Fihri, A.; Artero, V.; Razavet, M.; Baffert, C.; Leibl, W.; Fontecave, M. Cobaloxime-Based Photocatalytic Devices for Hydrogen Production. *Angew. Chem. Int. Ed.* **2008**, *47* (3), 564–567. <https://doi.org/10.1002/anie.200702953>.
- (19) Pfeffer, M. G.; Kowacs, T.; Wächtler, M.; Guthmüller, J.; Dietzek, B.; Vos, J. G.; Rau, S. Optimization of Hydrogen-Evolving Photochemical Molecular Devices. *Angew. Chem. Int. Ed.* **2015**, *54* (22), 6627–6631. <https://doi.org/10.1002/anie.201409442>.
- (20) Rau, S.; Schäfer, B.; Gleich, D.; Anders, E.; Rudolph, M.; Friedrich, M.; Görls, H.; Henry, W.; Vos, J. G. A Supramolecular Photocatalyst for the Production of Hydrogen and the Selective Hydrogenation of Toluene. *Angew. Chem. Int. Ed.* **2006**, *45* (37), 6215–6218. <https://doi.org/10.1002/anie.200600543>.
- (21) Pfeffer, M. G.; Schäfer, B.; Smolentsev, G.; Uhlig, J.; Nazarenko, E.; Guthmüller, J.; Kuhnt, C.; Wächtler, M.; Dietzek, B.; Sundström, V.; et al. Palladium versus Platinum: The Metal in the Catalytic Center of a Molecular Photocatalyst Determines the Mechanism of the Hydrogen Production with Visible Light. *Angew. Chem. Int. Ed.* **2015**, *54* (17), 5044–5048. <https://doi.org/10.1002/anie.201409438>.
- (22) Schulz, M.; Karnahl, M.; Schwalbe, M.; Vos, J. G. The Role of the Bridging Ligand in Photocatalytic Supramolecular Assemblies for the Reduction of Protons and Carbon Dioxide. *Coord. Chem. Rev.* **2012**, *256* (15), 1682–1705. <https://doi.org/http://dx.doi.org/10.1016/j.ccr.2012.02.016>.
- (23) Elvington, M.; Brown, J.; Arachchige, S. M.; Brewer, K. J. Photocatalytic Hydrogen Production from Water Employing A Ru, Rh, Ru Molecular Device for Photoinitiated Electron Collection. *J. Am. Chem. Soc.* **2007**, *129* (35), 10644–10645. <https://doi.org/10.1021/ja073123t>.
- (24) Chen, S.; Li, K.; Zhao, F.; Zhang, L.; Pan, M.; Fan, Y.-Z.; Guo, J.; Shi, J.; Su, C.-Y. A Metal-Organic Cage Incorporating Multiple Light Harvesting and Catalytic Centres for Photochemical Hydrogen Production. *Nat. Commun.* **2016**, *7* (1), 13169. <https://doi.org/10.1038/ncomms13169>.
- (25) Matt, B.; Fize, J.; Moussa, J.; Amouri, H.; Pereira, A.; Artero, V.; Izzet, G.; Proust, A. Charge Photo-Accumulation and Photocatalytic Hydrogen Evolution under Visible Light at an Iridium(III)-Photosensitized Polyoxotungstate. *Energy Environ. Sci.* **2013**, *6* (6), 1504–1508. <https://doi.org/10.1039/c3ee40352a>.
- (26) Walsh, J. J.; Bond, A. M.; Forster, R. J.; Keyes, T. E. Hybrid Polyoxometalate Materials for Photo(Electro-) Chemical Applications. *Coord. Chem. Rev.* **2016**, *306*, Part, 217–234. <https://doi.org/http://dx.doi.org/10.1016/j.ccr.2015.06.016>.
- (27) Black, F. A.; Jacquart, A.; Toupalas, G.; Alves, S.; Proust, A.; Clark, I. P.; Gibson, E. A.; Izzet, G. Rapid Photoinduced Charge Injection into Covalent Polyoxometalate–Bodipy Conjugates. *Chem. Sci.* **2018**, *9* (25), 5578–5584. <https://doi.org/10.1039/C8SC00862K>.
- (28) Rausch, B.; Symes, M. D.; Chisholm, G.; Cronin, L. Decoupled Catalytic Hydrogen Evolution from a Molecular Metal Oxide Redox Mediator in Water Splitting. *Sci.* **2014**, *345* (6202), 1326–1330. <https://doi.org/10.1126/science.1257443>.
- (29) Bloor, L. G.; Solarzka, R.; Bienkowski, K.; Kulesza, P. J.; Augustynski, J.; Symes, M. D.; Cronin, L. Solar-Driven Water Oxidation and Decoupled Hydrogen Production Mediated by an Electron-Coupled-Proton Buffer. *J. Am. Chem. Soc.* **2016**,

- 138 (21), 6707–6710.
<https://doi.org/10.1021/jacs.6b03187>.
- (30) Cronin, L.; Müller, A. POM-Themed Issue. **2012**, *41* (22), 7325–7648. <https://doi.org/10.1039/C2cs90087d>.
- (31) Anyushin, A. V.; Kondinski, A.; Parac-Vogt, T. N. Hybrid Polyoxometalates as Post-Functionalization Platforms: From Fundamentals to Emerging Applications. *Chem. Soc. Rev.* **2020**, *49* (2), 382–432. <https://doi.org/10.1039/C8CS00854J>.
- (32) Proust, A.; Matt, B.; Villanneau, R.; Guillemot, G.; Gouzerh, P.; Izzet, G. Functionalization and Post-Functionalization: A Step towards Polyoxometalate-Based Materials. *Chem. Soc. Rev.* **2012**, *41* (22), 7605–7622. <https://doi.org/10.1039/c2cs35119f>.
- (33) Streb, C. New Trends in Polyoxometalate Photoredox Chemistry: From Photosensitisation to Water Oxidation Catalysis. *Dalton Trans.* **2012**, *41* (6), 1651. <https://doi.org/10.1039/c1dt11220a>.
- (34) Lv, H.; Geletii, Y. V.; Zhao, C.; Vickers, J. W.; Zhu, G.; Luo, Z.; Song, J.; Lian, T.; Musaev, D. G.; Hill, C. L. Polyoxometalate Water Oxidation Catalysts and the Production of Green Fuel. *Chem. Soc. Rev.* **2012**, *41* (22), 7572–7589. <https://doi.org/10.1039/c2cs35292c>.
- (35) Sartorel, A.; Carraro, M.; Toma, F. M.; Prato, M.; Bonchio, M. Shaping the Beating Heart of Artificial Photosynthesis: Oxygenic Metal Oxide Nano-Clusters. *Energy Environ. Sci.* **2012**, *5* (2), 5592–5603. <https://doi.org/10.1039/c2ee02838g>.
- (36) Song, Y.-F.; Tsunashima, R. Recent Advances on Polyoxometalate-Based Molecular and Composite Materials. *Chem. Soc. Rev.* **2012**, *41* (22), 7384. <https://doi.org/10.1039/c2cs35143a>.
- (37) Izzet, G.; Volatron, F.; Proust, A. Tailor-Made Covalent Organic-Inorganic Polyoxometalate Hybrids: Versatile Platforms for the Elaboration of Functional Molecular Architectures. *Chem. Rec.* **2017**, *17* (2), 250–266. <https://doi.org/10.1002/tcr.201600092>.
- (38) Kibler, A. J.; Newton, G. N. Tuning the Electronic Structure of Organic-Inorganic Hybrid Polyoxometalates: The Crucial Role of the Covalent Linkage. *Polyhedron* **2018**, *154*, 1–20. <https://doi.org/https://doi.org/10.1016/j.poly.2018.06.027>.
- (39) Blazevic, A.; Rompel, A. The Anderson–Evans Polyoxometalate: From Inorganic Building Blocks via Hybrid Organic–Inorganic Structures to Tomorrows “Bio-POM.” *Coord. Chem. Rev.* **2016**, *307*, Part, 42–64. <https://doi.org/http://dx.doi.org/10.1016/j.ccr.2015.07.001>.
- (40) Schönweiz, S.; Rommel, S. A.; Kübel, J.; Micheel, M.; Dietzek, B.; Rau, S.; Streb, C. Covalent Photosensitizer–Polyoxometalate-Catalyst Dyads for Visible-Light-Driven Hydrogen Evolution. *Chem. Eur. J.* **2016**, *22* (34), 12002–12005. <https://doi.org/10.1002/chem.201602850>.
- (41) Hampson, E.; Cameron, J. M.; Amin, S.; Kyo, J.; Watts, J. A.; Oshio, H.; Newton, G. N. Asymmetric Hybrid Polyoxometalates: A Platform for Multifunctional Redox-Active Nanomaterials. *Angew. Chem. Int. Ed.* **2019**, *58* (50), 18281–18285. <https://doi.org/10.1002/anie.201912046>.
- (42) Al-Allaf, T. A. K.; Rashan, L. J.; Abu-Surrah, A. S.; Fawzi, R.; Steimann, M. Chemical Properties and Cytotoxic Activity of Complexes of Platinum(II) and Palladium(II) Containing DmsO and Various Anions; Synthesis and Structural Characterization of [Pt(DmsO)₂{O₂(CO)₂CCH₂CH₂CH₂}. *Transit. Met. Chem.* **1998**, *23* (4), 403–406. <https://doi.org/10.1023/A:1006942125847>.
- (43) Kowacs, T.; O'Reilly, L.; Pan, Q.; Huijser, A.; Lang, P.; Rau, S.; Browne, W. R.; Pryce, M. T.; Vos, J. G. Subtle Changes to Peripheral Ligands Enable High Turnover Numbers for Photocatalytic Hydrogen Generation with Supramolecular Photocatalysts. *Inorg. Chem.* **2016**, *55* (6), 2685–2690. <https://doi.org/10.1021/acs.inorgchem.5b01752>.
- (44) Luo, Y.; Maloul, S.; Wächter, M.; Winter, A.; Schubert, U. S.; Streb, C.; Dietzek, B. Is Electron Ping-Pong Limiting the Catalytic Hydrogen Evolution Activity in Covalent Photosensitizer–Polyoxometalate Dyads? *Chem. Commun.* **2020**, *56* (72), 10485–10488. <https://doi.org/10.1039/D0CC04509H>.
- (45) Ohsawa, Y.; Sprouse, S.; King, K. A.; DeArmond, M. K.; Hanck, K. W.; Watts, R. J. Electrochemistry and Spectroscopy of Ortho-Metalated Complexes of Iridium(III) and Rhodium(III). *J. Phys. Chem.* **1987**, *91* (5), 1047–1054. <https://doi.org/10.1021/j100289a009>.
- (46) Schönweiz, S.; Heiland, M.; Anjass, M.; Jacob, T.; Rau, S.; Streb, C. Experimental and Theoretical Investigation of the Light-Driven Hydrogen Evolution by Polyoxometalate-Photosensitizer Dyads. *Chem. Eur. J.* **2017**, *23* (61), 15370–15376. <https://doi.org/10.1002/chem.201702116>.
- (47) Schönweiz, S.; Knoll, S.; Anjass, M.; Braumüller, M.; Rau, S.; Streb, C. Electronic Supplementary Information for “CLICKable” Azide-Functionalized Phosphonates for the Surface-Modification of Molecular and Solid-State Metal Oxides.
- (48) Luo, Y.; Maloul, S.; Schönweiz, S.; Wächter, M.; Streb, C.; Dietzek, B. Yield—Not Only Lifetime—of the Photoinduced Charge-Separated State in Iridium Complex–Polyoxometalate Dyads Impact Their Hydrogen Evolution Reactivity. *Chem. – A Eur. J.* **2020**, *26* (36), 8045–8052. <https://doi.org/10.1002/chem.202000982>.
- (49) Hockin, B. M.; Li, C.; Robertson, N.; Zysman-Colman, E. Photoredox Catalysts Based on Earth-Abundant Metal Complexes. *Catal. Sci. Technol.* **2019**, *9* (4), 889–915. <https://doi.org/10.1039/C8CY02336K>.
- (50) Neubauer, A.; Grell, G.; Friedrich, A.; Bokarev, S. I.; Schwarzbach, P.; Gärtner, F.; Surkus, A.-E.; Junge, H.; Beller, M.; Kühn, O.; et al. Electron- and Energy-Transfer Processes in a Photocatalytic System Based on an Ir(III)-Photosensitizer and an Iron Catalyst. *J. Phys. Chem. Lett.* **2014**, *5* (8), 1355–1360. <https://doi.org/10.1021/jz5004318>.
- (51) Collins, F. C.; Kimball, G. E. Diffusion-Controlled Reaction Rates. *J. Colloid Sci.* **1949**, *4* (4), 425–437. [https://doi.org/10.1016/0095-8522\(49\)90023-9](https://doi.org/10.1016/0095-8522(49)90023-9).
- (52) Kiefer, L. M.; Kubarych, K. J. Solvent Exchange in Preformed Photocatalyst-Donor Precursor Complexes Determines Efficiency. *Chem. Sci.* **2018**, *9* (6), 1527–1533. <https://doi.org/10.1039/C7SC04533F>.
- (53) Neese, F. Software Update: The ORCA Program System, Version 4.0. *Wiley Interdiscip. Rev. Comput. Mol. Sci.* **2018**, *8* (1). <https://doi.org/10.1002/wcms.1327>.
- (54) Grimme, S.; Brandenburg, J. G.; Bannwarth, C.; Hansen, A. Consistent Structures and Interactions by Density Functional Theory with Small Atomic Orbital Basis Sets. *J. Chem. Phys.* **2015**, *143* (5), 054107. <https://doi.org/10.1063/1.4927476>.
- (55) Perdew, J. P.; Ernzerhof, M.; Burke, K. Rationale for Mixing Exact Exchange with Density Functional Approximations. *J. Chem. Phys.* **1996**, *105* (22), 9982–9985. <https://doi.org/10.1063/1.472933>.
- (56) Adamo, C.; Barone, V. Toward Reliable Density Functional Methods without Adjustable Parameters: The PBE0 Model. *J. Chem. Phys.* **1999**, *110* (13), 6158–6170. <https://doi.org/10.1063/1.478522>.
- (57) Weigend, F.; Ahlrichs, R. Balanced Basis Sets of Split Valence, Triple Zeta Valence and Quadruple Zeta Valence Quality for H to Rn: Design and Assessment of Accuracy. *Phys. Chem. Chem. Phys.* **2005**, *7* (18), 3297. <https://doi.org/10.1039/b508541a>.
- (58) Eichkorn, K.; Weigend, F.; Treutler, O.; Ahlrichs, R. Auxiliary Basis Sets for Main Row Atoms and Transition Metals and Their Use to Approximate Coulomb Potentials. *Theor. Chem. Accounts Theory, Comput. Model. (Theoretica Chim. Acta)* **1997**, *97* (1–4), 119–124. <https://doi.org/10.1007/s002140050244>.
- (59) Andrae, D.; Häußermann, U.; Dolg, M.; Stoll, H.; Preuß, H. Energy-Adjusted ab Initio Pseudopotentials for the Second and Third Row Transition Elements: Molecular Test for M₂ (M=Ag, Au) and MH (M=Ru, Os). *Theor. Chim. Acta* **1991**, *78* (4), 247–266. <https://doi.org/10.1007/BF01112848>.
- (60) Grimme, S.; Antony, J.; Ehrlich, S.; Krieg, H. A Consistent and Accurate Ab Initio Parametrization of Density Functional

- Dispersion Correction (DFT-D) for the 94 Elements H-Pu. *J. Chem. Phys.* **2010**, *132* (15), 154104. <https://doi.org/10.1063/1.3382344>.
- (61) Grimme, S.; Ehrlich, S.; Goerigk, L. Effect of the Damping Function in Dispersion Corrected Density Functional Theory. *J. Comput. Chem.* **2011**, *32* (7), 1456–1465. <https://doi.org/10.1002/jcc.21759>.
- (62) Cossi, M.; Rega, N.; Scalmani, G.; Barone, V. Energies, Structures, and Electronic Properties of Molecules in Solution with the C-PCM Solvation Model. *J. Comput. Chem.* **2003**, *24* (6), 669–681. <https://doi.org/10.1002/jcc.10189>.
- (63) Hirshfeld, F. L. Bonded-Atom Fragments for Describing Molecular Charge Densities. *Theor. Chim. Acta* **1977**, *44* (2), 129–138. <https://doi.org/10.1007/BF00549096>.
- (64) Fukui, K.; Yonezawa, T.; Shingu, H. A Molecular Orbital Theory of Reactivity in Aromatic Hydrocarbons. *J. Chem. Phys.* **1952**, *20* (4), 722–725. <https://doi.org/10.1063/1.1700523>.
- (65) Parr, R. G.; Yang, W. Density Functional Approach to the Frontier-Electron Theory of Chemical Reactivity. *J. Am. Chem. Soc.* **1984**, *106* (14), 4049–4050. <https://doi.org/10.1021/ja00326a036>.
- (66) Heussner, K.; Peuntinger, K.; Rockstroh, N.; Nye, L. C.; Ivanovic-Burmazovic, I.; Rau, S.; Streb, C. Solution and Solid-State Interactions in a Supramolecular Ruthenium Photosensitizer-Polyoxometalate Aggregate. *Chem. Commun. (Camb)*. **2011**, *47* (24), 6852–6854. <https://doi.org/10.1039/c1cc11859e>.
- (67) De Pascali, S. A.; Migoni, D.; Papadia, P.; Muscella, A.; Marsigliante, S.; Ciccarese, A.; Fanizzi, F. P. New Water-Soluble Platinum(II) Phenanthroline Complexes Tested as Cisplatin Analogues: First-Time Comparison of Cytotoxic Activity between Analogous Four- and Five-Coordinate Species. *Dalton Trans.* **2006**, *2* (42), 5077–5087. <https://doi.org/10.1039/b610945d>.
- (68) González, M.; Bartolomé, R.; Matarraz, S.; Rodríguez-Fernández, E.; Manzano, J. L.; Pérez-Andrés, M.; Orfao, A.; Fuentes, M.; Criado, J. J. Platinum Complexes for Multi-Parametric Assays Using Microarray Systems. *J. Inorg. Biochem.* **2012**, *106* (1), 43–45. <https://doi.org/10.1016/j.jinorgbio.2011.08.015>.
-